LAWRENCE
LIVERMORE
NATIONAL
LABORATORY

LLNL-TR-411183

Mitigation of Electromagnetic Pulse (EMP) Effects from Short-Pulse Lasers and Fusion Neutrons

D. C. Eder, A. Throop, C. G. Brown, Jr., J. Kimbrough, M. L. Stowell, D. A. White, P. Song, N. Back, A. MacPhee, H. Chen, W. DeHope, Y. Ping, B. Maddox, J. Lister, G. Pratt, T. Ma, Y. Tsui, M. Perkins, D. O'Brien, P. Patel

March 10, 2009

Disclaimer

This document was prepared as an account of work sponsored by an agency of the United States government. Neither the United States government nor Lawrence Livermore National Security, LLC, nor any of their employees makes any warranty, expressed or implied, or assumes any legal liability or responsibility for the accuracy, completeness, or usefulness of any information, apparatus, product, or process disclosed, or represents that its use would not infringe privately owned rights. Reference herein to any specific commercial product, process, or service by trade name, trademark, manufacturer, or otherwise does not necessarily constitute or imply its endorsement, recommendation, or favoring by the United States government or Lawrence Livermore National Security, LLC. The views and opinions of authors expressed herein do not necessarily state or reflect those of the United States government or Lawrence Livermore National Security, LLC, and shall not be used for advertising or product endorsement purposes.

Auspices Statement

This work performed under the auspices of the U.S. Department of Energy by Lawrence Livermore National Laboratory under Contract DE-AC52-07NA27344. This work was funded by the Laboratory Directed Research and Development Program at LLNL under project tracking code 06-ERD-055.

FY08 LDRD Final Report
Mitigation of Electromagnetic Pulse (EMP) Effects from Short-Pulse Lasers and Fusion Neutrons
LDRD Project Tracking Code: 06-ERD-055
David Eder, Principal Investigator

Abstract
Our research focused on obtaining a fundamental understanding of the source and properties of EMP at the Titan PW(petawatt)-class laser facility. The project was motivated by data loss and damage to components due to EMP, which can limit diagnostic techniques that can be used reliably at short-pulse PW-class laser facilities. Our measurements of the electromagnetic fields, using a variety of probes, provide information on the strength, time duration, and frequency dependence of the EMP. We measure electric field strengths in the 100's of kV/m range, durations up to 100 ns, and very broad frequency response extending out to 5 GHz and possibly beyond. This information is being used to design shielding to mitigate the effects of EMP on components at various laser facilities. We showed the need for well-shielded cables and oscilloscopes to obtain high quality data. Significant work was invested in data analysis techniques to process this data. This work is now being transferred to data analysis procedures for the EMP diagnostics being fielded on the National Ignition Facility (NIF). In addition to electromagnetic field measurements, we measured the spatial and energy distribution of electrons escaping from targets. This information is used as input into the 3D electromagnetic code, EMSolve, which calculates time dependent electromagnetic fields. The simulation results compare reasonably well with data for both the strength and broad frequency bandwidth of the EMP. This modeling work required significant improvements in EMSolve to model the fields in the Titan chamber generated by electrons escaping the target. During dedicated Titan shots, we studied the effects of varying laser energy, target size, and pulse duration on EMP properties. We also studied the effect of surrounding the target with a thick conducting sphere and cube as a potential mitigation approach. System generated EMP (SGEMP) in coaxial cables does not appear to be a significant at Titan. Our results are directly relevant to planned short-pulse ARC (advanced radiographic capability) operation on NIF.

I. Introduction/Background

Properties of EMP generated in laser facilities depend on the pulse duration, energy, and intensity of the laser. For lasers with nanosecond pulses, laser-plasma interactions can produce "hot electrons" in the 10 to 100 keV range. The number and energy of these hot electrons is usually inferred from the hard x-rays produced when these electron interact with the target material. Only a small fraction of these hot electrons escape the target because of large electrostatic fields associated with these escaping electrons. The dominant source of EMP at these laser facilities is due to these escaping electrons. The level of EMP is generally the greatest for large targets, with a potential reason being a

reduced electrostatic field associated with the larger surface area allowing more electrons to escape. When these facilities are used to generate significant fusion yield, the resulting neutrons generate large gamma fluences as they pass through the target chamber and other objects in the target bay. These gammas can produce Compton electrons and SGEMP in cables and other electronics.

At PW-class lasers facilities with picosecond laser pulses, the problems with EMP are particularly acute, where measurements of the unique physical phenomena produced at these facilities are often hampered by EMP. In the 10+ years since the petawatt threshold was crossed, a number of short-pulse PW-class lasers have been built around the world. A new short-pulse PW-class laser at LLNL, Titan, had its first shots in 2005. At the 5th International Laser Operations Workshop held at LLNL in September 2005, the need for a better understanding of EMP in PW-class laser facilities was clearly stated. Researchers reported many cases of EMP-induced diagnostic damage and data loss at each of the six PW-class laser facilities represented.[1] Empirical mitigation techniques involving isolation and shielding have not worked reliably. There was concern expressed that EMP would be a serious problem on the next generation of PW-class lasers with significantly more energy, e.g., Omega-EP at Rochester and ARC operation on NIF at Livermore. This concern provided motivation for this 3 year LDRD, which started in FY06.

Short-pulse, PW-class lasers produce very energetic (MeV) electrons and because of their high energy more can escape from the target. Even in the case of short-pulse lasers, the number of electrons that escape (~10^{12}) is a small fraction of the total number produced in the target, and the associated charge is a small fraction of a Coulomb. However, the short duration can produce very large transient currents and large EMP. In addition, the short impulse of electrons has a correspondingly broad spectrum with the potential of high (GHz) frequency EMP. For effective shielding it is critical that the frequency of the EMP is known. Previous researchers have made measurements of EMP at short-pulse PW-class laser facilities with a focus on chamber modes.[2] In this paper, it was proposed that the measured EMP is associated with high-energy electrons that escape from the target. However, there were no measurements that showed a clear correlation of EMP with electron number. As part of our LDRD research, we undertook an effort to measure the electromagnetic fields inside and outside a short-pulse laser chamber as well as the spatial and energy distribution of the escaping electrons. To measure electron energy as well as information on the spatial distribution of escaping electrons we built on previously funded LDRD research using compact electron spectrometers.[3] Techniques using image plates and other detectors provided additional information on the escaping electrons as discussed in the following sections.

II. Research Activities

Our research focused on obtaining a fundamental understanding of the source and properties of EMP at short-pulse, PW-class laser facilities. We did ride-along measurements and conducted dedicated shots on the Titan short-pulse PW-class laser, which is a part of the Jupiter Laser Facility at LLNL. Our research activities can be grouped into four general areas: 1) measurement of EMP, 2) measurement of escaping

electrons, 3) data analysis of EMP data, and 4) simulations of EMP. Fundamental research was required in each of these areas to obtain the results discussed in this report.

Measurement of EMP

In order to characterize the EMP inside and outside of the Titan laser chamber a wide range of field probes is required. The electric and magnetic fields are measured separately using D-dot and B-dot probes, respectively. (It is important to measure both the magnetic and electric fields because the ratio of the fields generally is not the free-space value inside resonant chambers.) The requirement to measure a wide frequency spectrum from 50 MHz to 5 GHz, mandates multiple probes of various sizes. In Figure 1, we show a large, low-frequency B-dot (RB-50) probe, a smaller, mid-frequency B-dot (RB-270) probe, and two small, high-frequency B-dot (RB-230) probes (horizontal and vertical orientations) located inside the Titan laser chamber. These B-dot probes have conducting loops that generate a current as the magnetic field through the loop is varied. A mid-frequency D-dot (AD-55) probe is shown in Figure 2, where the two asymptotic sensing elements located on opposite sides of a common ground plate are evident. These B-dot and D-dot probes are commercial (Prodyn) probes that have been designed to work in high-radiation environments. The B-dot probes use a moebius pickoff and both types use baluns to reject common-mode noise. We employed a photodiode to discern the arrival of the laser pulse. The probe outputs are digitized by 10 and 20 Gsample/s oscilloscopes. (The faster oscilloscopes are used for the high-frequency probes and the digitization rate is what limits our measurement to ~5 GHz.)This was the first time many of these probes were used in a laser chamber, and it was not clear what level of shielding would be required for the cables and oscilloscopes to reduce background EMP noise. Initial measurements with the oscilloscopes located in a conventional enclosed rack in the same room as the laser chamber resulted in unacceptable noise levels. Measurement of local fields by the probes in a strong EMP environment requires careful and conservative grounding and shielding because other components of the measuring system, e.g., cables, oscilloscopes, etc., also respond to the EMP. We acquired a very well (100 dB) shielded enclosure for the oscilloscopes (Figure 3) and located this enclosure in a neighboring room. The cables from the internal probes were placed in well-shielded (80 dB) solid conduit as they passed from the chamber into the shielded enclosure prior to being connected to the oscilloscopes.

Measurement of Escaping Electrons

An important part of this research is to establish the connection between escaping electrons and EMP, which requires measurements of the number of electrons and their spatial distribution. We also measured the energy distribution, which is valuable data for people modeling the electron dynamics inside the targets and designing electron deflection packages for diagnostics. We obtain electron information from compact electron spectrometers, TLD's (ThermoLuminescent Detectors), UTLD's (Ultrathin TLD's), image plates, and a Faraday cup with fast and integrating current sensors. We fielded seven low-energy (out to 4 MeV) compact electron spectrometers at various angles inside the Titan chamber. We were able to absolutely calibrate these detectors using a combination of Monte Carlo simulations and off-line experiments. In addition, we fielded one high-energy (out to 100 MeV) compact electron spectrometer. We fielded

28 TLD's in groups of 4 around the Titan chamber. For each group of 4, one was unshielded, one had a shielded cap that is design to give flat response to radiation as a function of energy, one had cap plus a thin shield, and one had cap plus thicker shield. This combination in conjunction with Monte Carlo modeling allows one to separate the gamma and electron contribution to the dose and gives limited information on electron energy. The UTLD's are more sensitive to electrons than gammas and were fielded as an array on one of our larger image plates and at other locations in the chamber. The large image plate was fielded to measure evidence of a directed beam of escaping electrons. Additional image plates gave information on the spatial distribution of escaping electrons. Finally, a well-shielded Faraday cup provided information on number of electrons striking the cup. In Figure 4, we show three low-energy compact electron spectrometers, one high-energy compact electron spectrometer, three groupings of 4 TLD's, and the Faraday cup located in the Titan chamber. In Figure [5], we show the large image plate with an array of UTLD's. (These UTLD's were covered with a thin Al layer prior to most shots.) In Figure [6], we show the large image plate with plastic steps used to distinguish electrons from gammas.

Data Analysis of EMP Data

As stated earlier, the D- and B-dot probes do not measure the electric and magnetic fields directly as a function of time. Instead, the output voltage measured at their terminals is the time derivative (also called the *transfer function*) of the actual time variation of the electric and magnetic fields. The transfer function must be inverted and applied to the measured probe output voltages in order to obtain the fields, which is a process called *deconvolution*. We perform deconvolution on the output voltage measurements using simple transfer functions derived from [4] and [5] and adjusted for attenuation in the measurement system. Since deconvolution using the transfer functions of our probes greatly amplifies low-frequency noise, we high-pass filter the resulting signal to dampen the low-frequency noise. See [6] for an additional, more complex approach we have used to deal with the low-frequency noise amplification problem. Further, we have developed and implemented an adaptive filtering technique to reduce noise in measurements due to direct interaction of electrons, x-rays, etc. with the probes and their cables. The resulting electric and magnetic field time series can be further processed and displayed for visualization purposes. Our data visualization products include time-series plots, displays of spectra, and images of spectrograms, showing how the spectrum of a signal changes with time. See [7] for a more detailed description of our signal processing and visualization algorithms.

Simulations of EMP

The Titan laser target chamber is roughly cylindrical with a height of nearly one meter and a radius of one meter. The chamber also has several portholes for diagnostic equipment as well as the input port for the laser beam. We are primarily interested in the pulse of electromagnetic waves radiated by a charge packet associated with electrons leaving the target. Also, we do not currently attempt to model the charge packet as a plasma, it is simply a known charge density moving through the mesh in a prescribed fashion. This approximation is valid for this particular problem because the liberated electrons have very high energies. For these simulations we use the 3D electromagnetic

code EMSolve, which has been used for a wide range of applications. [8-14] However, to simulate EMP in the Titan chamber we had to change from the standard E/B formulation for solving Maxell equations to a D/H formulation as discussed below.

Maxwell equations are commonly discretized using “edge-elements”, or discrete 1-forms, for the electric field and “face-elements”, or discrete 2-forms, for the magnetic flux density. However, this scheme does have certain drawbacks. One difficulty with 1-form current densities is that they can spread through material interfaces into non-physical regions. Another difficulty, and the one we will focus on, arises if the current density is transient and the primary interest is to determine how a cavity will resonate after a current pulse passes through it. The problem here is that the continuity equation for the electric charge is only weakly satisfied. Therefore, current densities can, and often do, leave behind non-physical charge densities after they pass through the computational mesh.

The standard E/B formulation of the problem requires that current be approximated by discrete 1-forms with degrees of freedom on the edges of the mesh. The divergence of a 1-form can only be defined in a weak sense, i.e., as a type of least squares best fit. Hence the continuity equation for the electric charge may not be locally satisfied everywhere although it should be nearly satisfied globally. Unfortunately, it also can result in a large non-physical charge buildup left behind in the wake of the packet. The boundary of the computational domain is assumed to be a perfect electrical conductor so the charge near the boundary can be interpreted as being related to the surface charge density. This is actually another oddity of the E/B formulation: surface charges appear smeared into the volume elements which touch the surface. This may not be an attractive feature of the image but at least it has a reasonable physical interpretation.

The non-physical charge buildup can be removed by performing divergence cleaning when deemed necessary or perhaps at every time step. This is the process of adding something to the field so that its divergence has a desired value but its curl remains unchanged. For the model problem we can add some additional current to the source so that the divergence will match the desired change in charge density. We assume that the correction to the current is the gradient of a scalar field so that it will have zero curl. Each divergence cleaning operation then requires an additional linear solve to compute the scalar field. Unfortunately, this method has a drawback when the charge density has a velocity near the speed of light. The correction introduces a small quasi-static field centered on the charge density, which appears to propagate faster than the speed of light. Figure [7] shows a logarithmically scaled contour plot of the electric field magnitude, which clearly shows contours well beyond the charge packet, which is located near the innermost contour. This component of the field can also be seen because it introduces surface charge densities on the metal object ahead of the charge packet and on several sharp corners farther away. These non-physical charge densities are obviously due to the global solve necessary in the divergence cleaning computation.

We now discuss our new D/H formulation to solve Maxwell equations. The difficulties discussed so far stem from the treatment of the current as a 1-form vector field. Current

density is, however, a flux vector, i.e., the amount of charge crossing a given area per unit time. Flux vector fields are more naturally described using 2-forms so we should have more luck if we approximate Ampere's law using discrete 2-forms. In this formulation the curl of D must be computed in the weak sense. This weak form requires the solution of a linear system to update H using Faraday's law. In the standard E/B formulation it is the curl of B that must be computed in the weak sense, requiring a linear solve in Ampere's law to update E. Normally this linear solve allows us to apply voltage boundary conditions on E, where we can specify that the tangential component of E is zero on perfect electrical conductors. In the D/H formulation proposed here this constraint becomes unnecessary because the natural boundary condition is that the tangential component of the curl of H be zero but, of course, this is equivalent to E being zero on the boundary.

Simply treating the current as a 2-form does not magically solve all of our problems. What it does is convert our charge buildup problem from a global least-squares fit into much more simple local charge conservation problem. One way to solve this problem is to use a particle-in-cell (PIC) technique. We don't have the space to describe this procedure in detail but the essential idea is simple enough. Split up the trajectory of the charge packet into a group of rays and imagine the charges themselves as beads moving along these rays. Each time a bead crosses a cell boundary a small flux is applied to the corresponding face in the mesh. If enough rays are used and there are enough beads strung along each ray, then the source will appear reasonably smooth. We should emphasize that we are not performing a self-consistent PIC simulation. The fields do not affect the motion of the charge packet in any way. We are simply using the PIC concept as a bookkeeping scheme to maintain charge conservation.

Figure [8] again shows a logarithmically scaled contour plot of the electric field magnitude, analogous to that shown in Figure [7]. However, in the new plot the non-physical, quasi-static field contours are no longer present. The fields now properly propagate within a spherical shell, which expands at the speed of light. This work has been accepted for publication. [15] We now can use these simulation to predict the time varying electric and magnetic fields at any location in the chamber. These fields can then be directly compared with measurements using D-dot and B-dot probes.

III. Results/Technical Outcome

Measurement of EMP is challenging because it is critical to separate the EMP measured by the B-dot or D-dot probe from EMP picked up by cables, power cords, oscilloscopes, etc. As discussed above our initial placement of the oscilloscopes in an enclosed rack inside the room with the Titan chamber resulted in unacceptable EMP noise. To validate that our new well-shielded enclosure for the oscilloscopes located in a neighboring room and cable shielding were acceptable, we covered one of our B-dot probes with sufficiently thick Al foil to shield out EMP and compared this data with another shot with very similar target and laser parameters with the same probe unshielded. The result of this comparison is shown in Figure [9]. This results also provides evidence that system generated EMP (SGEMP) produced by gammas from the target is not a major source of noise. (Fusion neutrons during yield experiments at NIF will produce large gamma

fluences and subsequent SGEMP. As part of this LDRD, we established a collaboration with Sandia National Laboratory to study SGEMP and transferred two of their SGEMP codes to LLNL.)

Escaping Electrons and EMP

One of our primary goals was to clearly establish the connection between escaping electrons and EMP. There was speculation that radiation from the target (UV, x-rays, and gamma-rays) would produce photo electrons from surfaces in the chamber leading to another source of EMP. During our dedicated shots on Titan, we showed that the escaping electrons are the primary source of EMP and the contribution from radiation, if any, is minor. To demonstrate that electrons are the primary EMP source, we used thin (12 micron) Ag foil targets of varying size, while holding laser energy, pulse duration, spot size constant. We shot targets from 0.1 to 50 mm in size with a laser shot size of ~20 microns, which is small compared to even the smallest target. We observed that EMP signals and the number of escaping electrons increased with increasing target size. In contrast, we did not observe a significant change in radiation, as expected. In Figure [10], we show the EMP signal as a function of target size. (This data is from a D-Dot probe measuring out to ~2 GHz, so as discussed below, the actual EMP level could be approximately a factor of 2 higher because of high-frequency EMP not detected by this probe.) We have good data from the high-energy spectrometer for 4 of these shots with results shown in Figure [11], where we observe a clear increase in number of electrons, and we also see that the energy of the escaping electrons extends out to ~25 MeV. The increase in number of escaping electrons is believed due to the larger surface area resulting in a reduction of the electrostatic electric field on the target. If targets are made sufficient large, one would expect to see a roll off because of the finite duration of energetic electrons in the target. We see some evidence of this as we go to our largest (50 mm) target. That fact that we continue to see increasing EMP going from 10- to 50- mm target, implies that the duration of the energetic electrons must be of order 20 ps or longer. This is significantly longer than the laser pulse duration of 2 ps. These results combined with similar ones obtained at different laser pulse durations, establish a clear connection between EMP and escaping electrons as well as showing the benefit of using smaller targets.

Frequency Dependence of EMP

Another primary goal of our research was to measure the frequency dependence of the EMP. We focused our attention on the frequency range, 50 MHz to 5 GHz, where most diagnostics have significant sensitivity to EMP. To span this frequency range we use a series of B-dot and D-dot probes as already discussed. We perform deconvolution on the output voltage of these probes using transfer functions adjusted for attenuation in the measurement system. We high-pass filter the resulting signal to dampen the low-frequency noise introduced by the transfer functions. In Figure [12], we give the power spectral density as a function of frequency on a log-log scale using three B-dot probes. (These are the same B-dot probes shown in Figure [1].) There is reasonable agreement as we transition between the different probes. We give the measured noise level for each of these probes as dashed curves. An important point is the relatively slow fall off as we go to high frequency. In the same figure, we give the calculated spectral power density using

the EMSolve code using 5 x 10^{12} electrons leaving the target as input into the code. This number of electrons is consistent with our measurements discussed below. We see that there is quite good agreement with the strength of the EMP as well as reasonable agreement with the frequency dependence. To confirm the high-frequency nature of EMP on Titan, we did measurements where we placed a high-pass filter on the RB-230 B-dot probe that blocked the signal above 2 GHz and saw a factor of 2 reduction. This means that approximately 1/2 of the EMP is above 2 GHz, which has implications for the design of appropriate shielding of components in the chamber.

As shown in Figure [1], we place the high-frequency B-dot probes in horizontal and vertical orientations. In general, probes in the vertical orientation have higher peak fields than ones in the horizontal orientation. A potential explanation is that the magnetic field associated with an electron bunch moving past a probe is coupled more efficiently to one in the vertical orientation. This can also explain the rapid decay of the field in the vertical orientation, which is shown in the bottom plot of Figure [13]. We give the electric field as a function of time with a peak field of order 400 kV/m obtained from a B-dot probe (with approximate scaling by the speed of light to yield the electric field). In the upper plot we give the frequency dependence of the fields as a function of time. We see that the broad frequency content of the fields lasts for the duration of the EMP. In Figure [14], we give the corresponding results for data obtained from a B-dot probe in the horizontal orientation. We see that the peak field for this orientation is significant less with a slower decay.

The majority of EMP associated damage in laser experiments is for components located inside laser chambers, but computer upsets and other problems can occur for components outside the chamber. To understand the shielding effectiveness of the Titan laser chamber, we also measured the fields outside the chamber. In Figure [17], we show results for a B-dot probe located outside a Titan port window. There is a significant reduction in the fields, which is most pronounced for lower frequencies as shown in the upper spectrogram. If the EMP spectrum inside the chamber had extended only out to ~1 GHz, rather than the measured 5 GHz or higher, the EMP outside would have been reduced significantly more than what we measured on Titan. This shows the importance of knowing the frequency of the EMP generated inside the chamber.

Absolute Calibration of Electron Spectrometer

As part of this LDRD research, we contributed to the absolute calibration of the image plates (IP's) used in the low-energy (0.1-4 MeV) compact electron spectrometers. First the photon stimulated luminescence (PSL) of the IP was calibrated against absolutely calibrated UTLD's using electrons from the same electron source. (Electrons came from a target heated by a short-pulse laser.) The UTLD's were placed in holes cut into the IP that was placed inside the electron spectrometer. To deduce the number of electrons, we did Monte Carlo simulations using MCNPX, where we calculated the fraction of electron energy absorbed by the UTLD and IP material for each electron energy and incident angle defined by the spectrometer angle. The 3D model for the IP included the 9-micron thick polyethyleneterephthalate (PET) layer that is front of the 120-micron thick BaFBrI IP material as well as the backing material. This work has been recently published. [16]

Number and Spatial Distribution of Escaping Electrons

We measured the spatial dependence of the electrons using various methods as described above. The angular and energy dependence obtained from the absolutely calibrated low-energy compact spectrometers is shown in Figure [18]. The target for this shot was a square (1 mm by 1 mm), 12-micron thick Ag foil. For this plot, we grouped the energy dependence into 4 energy bins (100-250 keV, 0.25-1 MeV, 1-2 MeV, and 2-4 MeV). The seven compact spectrometers are located at various angles surrounding the target with 0 degrees corresponding to the laser-beam axis. The Ag foil is tilted 28 degrees to the laser axis, so the normal points to 332 degrees. We see from the figure that the spectrometer near that angle has the largest number of electrons. However, there is a significant number of electrons at all angles. The highest-energy electrons (2-4 MeV) are the most directional pointing along the rear surface normal. The solid angle of the entrance slit of the electron spectrometers is $\sim 10^{-5}$ steradian. The average number of electrons for all 4 energy bins is about 8×10^{11} electrons per steradian. If the distribution was isotropic, this corresponds to about 10^{13} electrons. From the high-energy spectrometer data, there can be comparable number of electrons with energy higher than 4 MeV. However, it appears that the majority of the electrons are emitted towards the equator of the target chamber and not towards the top and bottom of the chamber so the total number is likely closer to 5×10^{12} electrons. We get similar results for total number of electrons using data taken with the Faraday cup with corresponding assumptions on angular distribution. As discussed above, when this number of electrons is used as into the 3D EMSolve simulations the calculated EMP magnitude and frequency dependence is in agreement with our measurements.

Mitigation of EMP using Beam Dumps

We explored the potential of using electron beam dumps to reduce the magnitude of the EMP generated. Initial efforts used a planar beam dump located on the backside of the target. We then tried spherical and cubic beam dumps that surrounded the target with an opening for the laser beam. The planar beam dump had no significant effect on EMP, while the beam dumps that surrounded the target achieved a factor of ~3 reduction in EMP. To provide spatial information about the escaping electrons, we use a large image plate holder (Figure [5-6]) that had layers of image plates sandwiched between layers of Al to obtain energy information on the escaping electrons. The metal frame was grounded to the laser table allowing this structure to function as an electron beam dump. For many shots an electron beam was observed on the image plates (Figure [17]). We conducted a wide range of shots with the same target and very similar laser parameters with and without the large image plate holder inside the chamber. In all cases, there was no significant correlation of EMP levels with the placement of holder. One potential reason is that a significant fraction of the escaping electrons are not confined in a beam leaving the rear surface. In addition, electromagnetic fields generated as electrons leave the target are not blocked by a planar electron beam dump. We next considered beam dumps that surround the target. However, it is not possible to completely enclose a target to block escaping electrons and associated electromagnetic fields because there must be an opening for the laser to strike the target. In Figure [18] we show a thick Al sphere that surrounds that target with an opening for the target holder and the laser beam. We added

a Cu foil to provide a conducting return path for electrons stopped by the sphere to go back to the target. The 1.25-cm thick Al stops electrons out to ~5 MeV so the majority of the electrons are stopped. The result of using this "mitigation" sphere is shown in Figure [19], where we compare the measured EMP with and without the sphere. We see an approximately factor of 3 reduction in EMP. We also fielded a very thick Al cube (Figure [20]) that is calculated to block even the most energetic electrons and obtained similar results. Detailed EMSolve simulation of the mitigation cube indicates that a significant fraction of the electromagnetic fields generated inside the cavity escape though the opening.

Energy Scaling of EMP

Finally, we discuss energy scaling, which is important for scaling our results to higher energy PW-class laser systems such as Omega-EP and ARC operation on NIF. In Figure [21] we give results for the peak strength of the EMP as measured by a high frequency B-dot probe as a function of energy. We show results for 0.6, 2, and 20 ps laser pulse durations. We see a clear increase of EMP with increasing energy with peak electric fields strengths reaching ~400 kV/m for our highest energy shot. The scaling with intensity for fixed energy by changing pulse length is not so clear. The target for all these shots is a square (1 mm by 1 mm), 12-micron thick Ag foil. It appears that fields in the MV/m range are likely as PW-class lasers extend into the kJ energy range.

IV. Exit Plan

Our work on Titan provides the groundwork for an EMP diagnostic on NIF. We use B-dot and D-dot probes that were validated on our Titan shots. The data analysis to reduce the probe data developed for Titan is being converted into NIF's analysis software suite. Modeling of the NIF chamber with EMSolve has been used to determine the lower order modes of the chamber. We will be measuring the fields inside and outside the NIF chamber. The lessons learned on Titan with respect to shielding requirements for cables and oscilloscopes are being applied to the NIF design. In addition, our measurements of the frequency dependence of EMP are being used to guide the shielding of all components in the NIF chamber. We have provided probes and advice for EMP measurement efforts on Omega and Omega-EP. Our research developed an experimental and modeling capability that is important for NIF, and the effort is now being funded directly by NIF.

V. Summary

We obtained a fundamental understanding of the source and properties of EMP at the Titan PW(petawatt)-class laser facility. The source of EMP is high-energy (MeV) electrons escaping from the target. We showed that EMP can be reduced by using small targets. We measured the EMP from 50 MHz to 5 GHz and found that the frequency dependence of the EMP is very broad with ~1/2 the energy above 2 GHz. This information is critical in the design of effective shielding to mitigate the effect of EMP on components. We determined that mitigation by the use of electron beam dumps that surround the target provide a modest reduction in EMP. We measured the number of escaping electrons to be in the 10^{12} to 10^{13} range using electron spectrometers that were absolutely calibrated as part of this research. These numbers were confirmed by Faraday

cup data. When these electron numbers are used as input into 3D electromagnetic simulations, the calculated EMP strength is in agreement with measurements. These simulations required that Maxwell equations be solved by a new D/H formulation to remove unphysical fields. Based on our observed scaling of EMP with energy, electric fields in the MV/m range are likely during ARC operation on NIF. This places requirements on shielding in the NIF chamber for such operation. Our data on the spatial and energy dependence of escaping electrons provides important data for on-going research on electron dynamics inside short-pulse driven targets and can be used to design electron deflection packages for diagnostics on short pulse lasers, including NIF.

VI. Acknowledgements

Jim Candy and Brian Guidry provided guidance in measurement planning and signal processing. We thank the team at the Jupiter Laser Facility for their assistance in our Titan experiments, particularly Rich Combs, Rob Costa, Jim Bonlie, Dwight Price, and Roger Van Maren.

VII. References

[1] EMP Breakout Session: Chaired by D. Eder with input provided by R. Broyles, J. Schwarz, J. Nolan, M. Norman, A. M. Sautivet, J. Bonlie, R. Johnson, C. Danson, S. Morse, and D. Kehne (2005).
[2] Mead M J et al. 2004 Electromagnetic pulse generation within a petawatt laser target chamber *Rev. Sci. Instr.* 75 4225-7.
[3] H. Chen and S. C. Wilks, Evidence of enhanced effective hot electron temperatures in ultraintense laser-solid interactions due to reflexing, Laser and Particle Beams (2005), 23:4:411-416 Cambridge University Press
[4] Edgel W R Electric & magnetic field sensor application Prodyn application note 192 http://www.prodyntech.com/download/appnotes/ap192.pdf accessed September 2008
[5] Duncan Jr. P H 1974 Analysis of the Moebius loop magnetic field sensor *IEEE Trans. EMC* 16 83-9
[6] Brown Jr. C G., A. Throop, D. Eder, and J. Kimbrough, "Electromagnetic pulses at short-pulse laser facilities," *Journal of Physics: Conference Series*. Vol. 112, 032025.
[7] Brown Jr. C G., A. Thoop, D. Eder, J. Kimbrough, and W. DeHope, "Overview of the measurement system and signal processing for electromagnetic pulse measurements in the Titan short-pulse laser facility," in preparation.
[8] M. Stowell, B. Fasenfest, D. White, "Investigation of radar propagation in buildings: A 10 billion element FETD simulation," IEEE Trans. Ant. Prop., v56, n 8, pp. 2241-2250, 2008.
[9] D. White, J. Koning, R. Rieben, "Development and Application of Compatible Discretizations of Maxwell's Equations," in Compatible Discretization of Partial Differential Equations, Springer-Verlag series on Mathematics and its Applications, v.142, 2006.
[10] P. Castillo, R. Rieben and D. White, "FEMSTER: An Object Oriented Class Library of High-Order Discrete Differential Forms," ACM Transactions on Mathematical Software, v 31, n. 4, pp 425-457, 2006.

[11] R. Rieben, G. Rodrigue, D. White, “A high order mixed finite element method for solving the time dependent Maxwell equations on unstructured grids,” Journal of Computational Physics, v. 204, n. 4, pp. 490-519, 2005.
[12] A. Fisher, G. Rodrigue, D. White, “A generalized mass lumping technique for vector finite element solutions of the time dependent Maxwell equations,” IEEE Trans. Ant. Prop.,v. 53 n. 9, pp 2900-2910, 2005.
[13] P. Castillo, J. Koning, R. Rieben, D. White, “A discrete differential forms framework for computational electromagnetics,” Comp. Meth. Eng. Sci. Vol 5 No 4 pp 331-346, 2004.
[14] D. White, M. Stowell, “Full wave simulation of electromagnetic coupling effects in RF and mixed-signal ICs using a time-domain finite-element method,” IEEE Trans. Micro. Theory Tech., Vol 52, No. 5, pp 1040 -1414, 2004.
[15] M. L. Stowell, "Discretizing Transient Current Densities in the Maxwell Equations," The 25th International Review of Progress in Applied Computational Electromagnetics, ACES 2009, Monterey, CA, USA, 8-12 March 2009.
[16] H. Chen, N. L. Back, T. Bartal, F. N. Beg, D. C. Eder. A. J. Link, A. G. MacPhee, Y. Ping, P. M. Song, A. Throop, and L. Van Woerkom, “Absolute Calibration of Image Plates for Electrons at Energy Between 100 keV and 4 MeV, Rev. Sci. Instrum. 79, 033301 (2008).

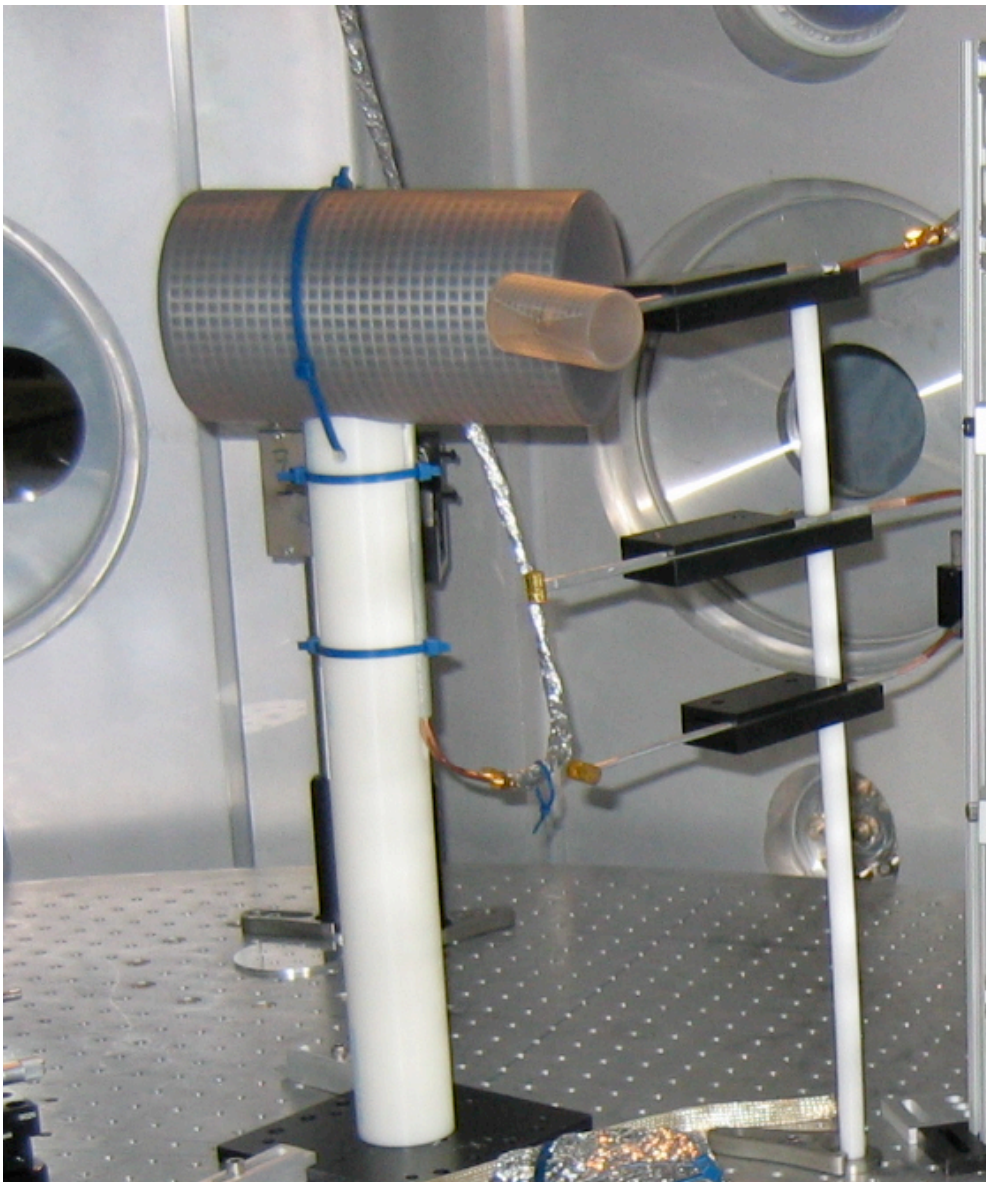

Figure 1: A low-frequency, a med-frequency, and two high-frequency B-dot probes are shown inside the Titan laser chamber.

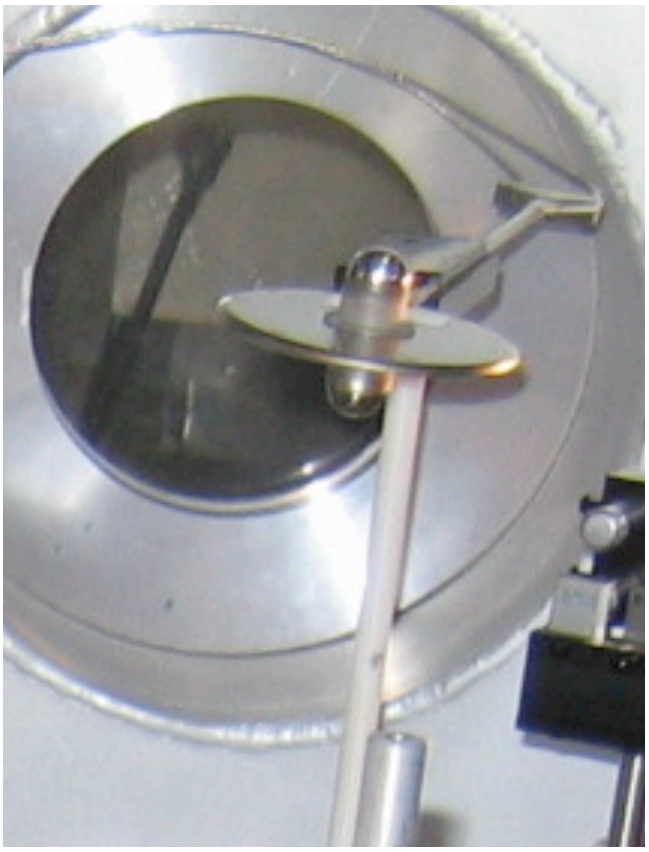

Figure 2: A med-frequency D-dot probe is shown inside the Titan laser chamber.

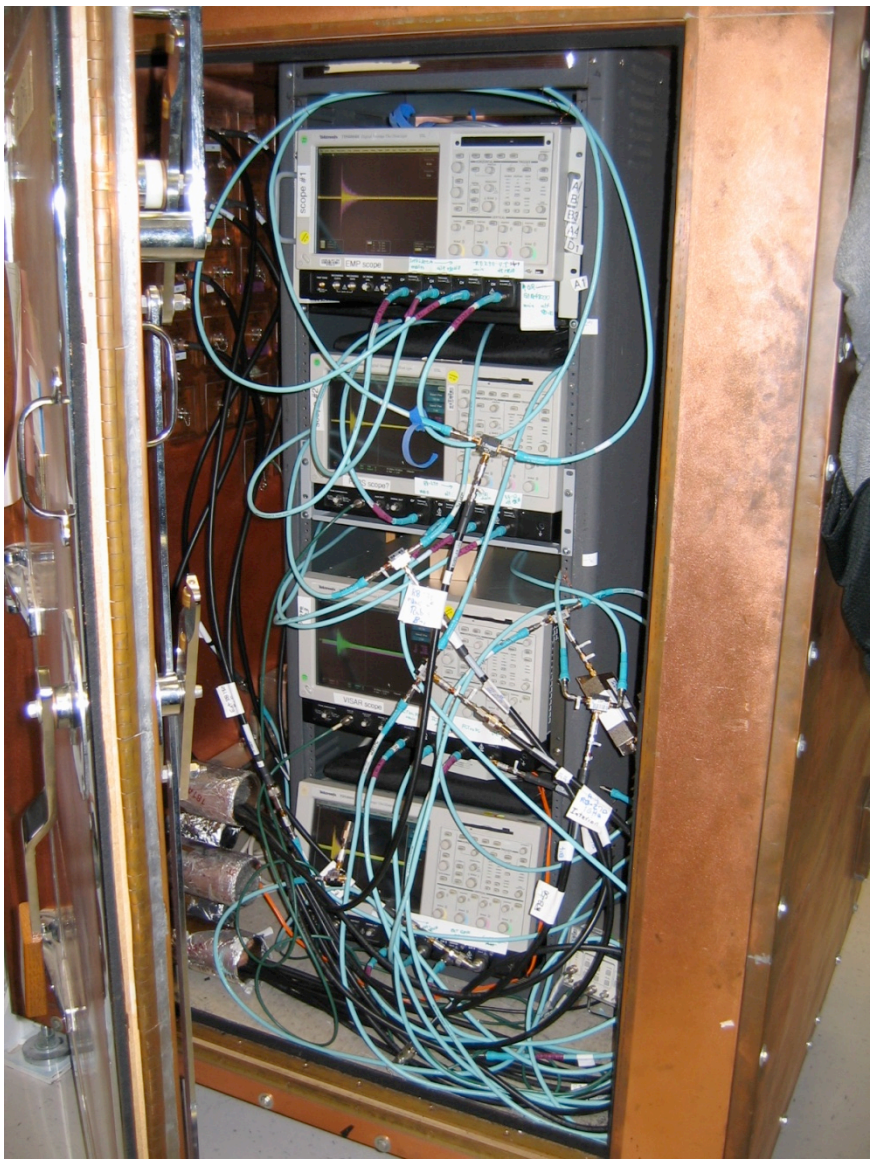

Figure 3: The well-shielded (100 dB) enclosure with four oscilloscopes is shown.

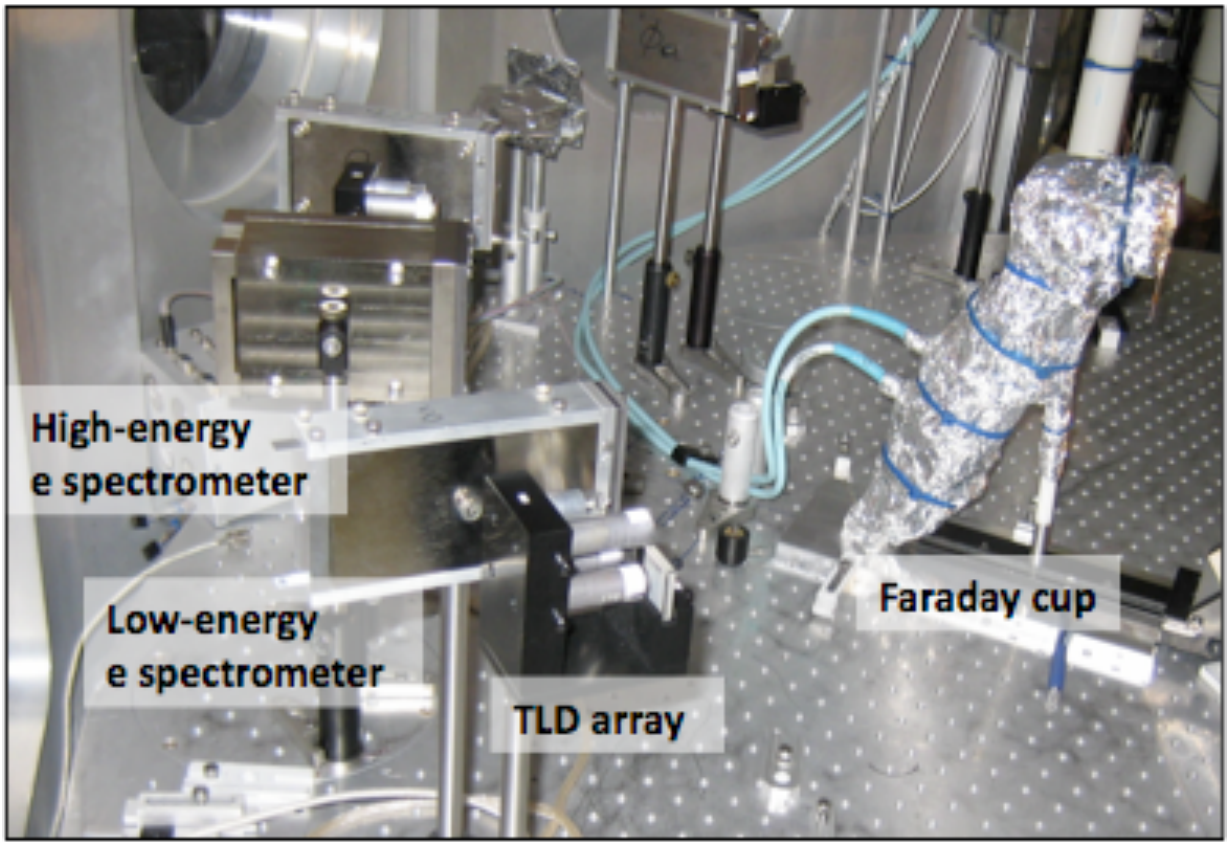

Figure 4: The escaping electrons are measured by various ways including a Faraday cup, a number of TLD arrays, a number of low-energy electron spectrometers, and a high-energy electron spectrometer.

Figure 5: The large image plate holder is shown with an array of UTLD's.

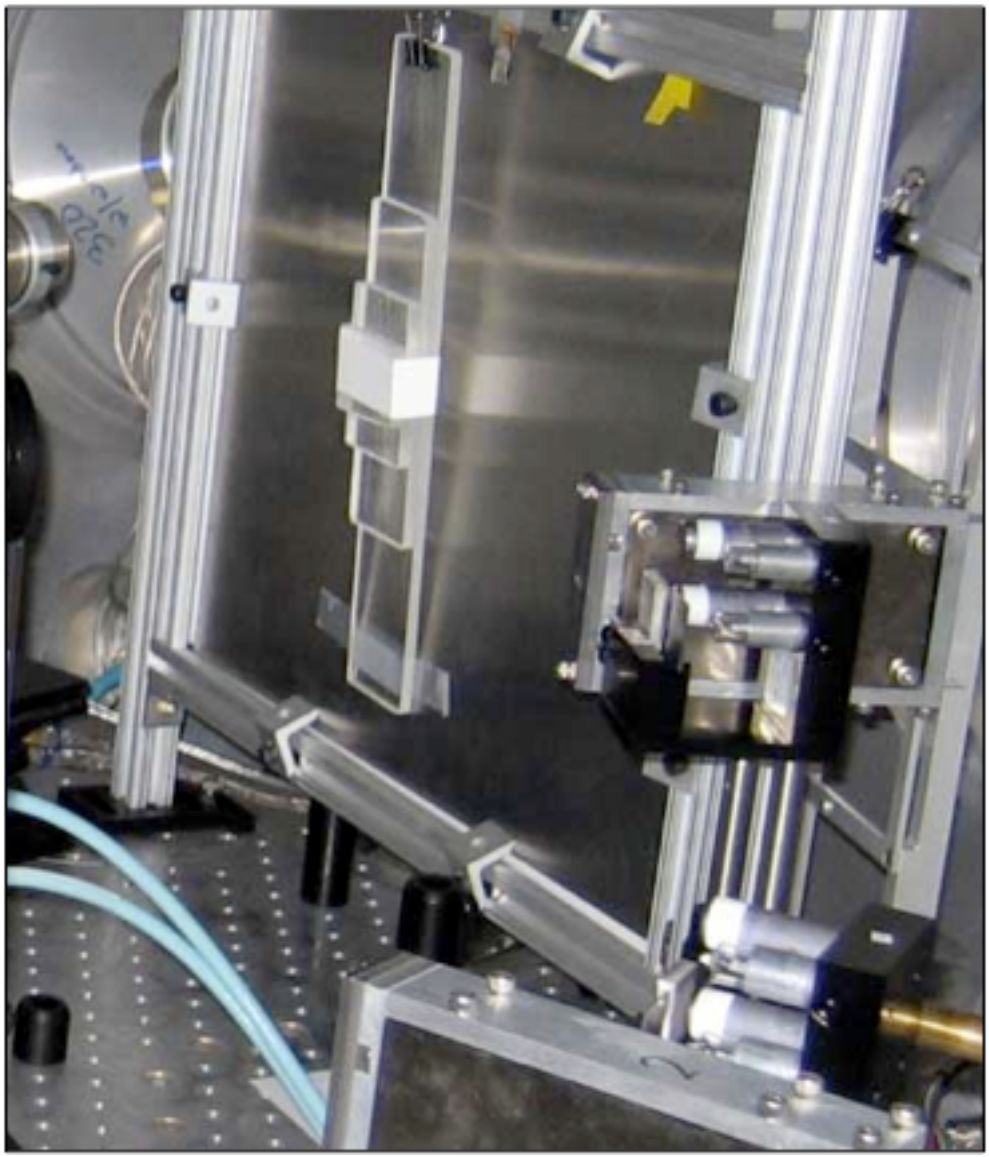

Figure 6: Large image plate holder with stepped plastic to determine relative contribution of electrons and gammas to plate explosure.

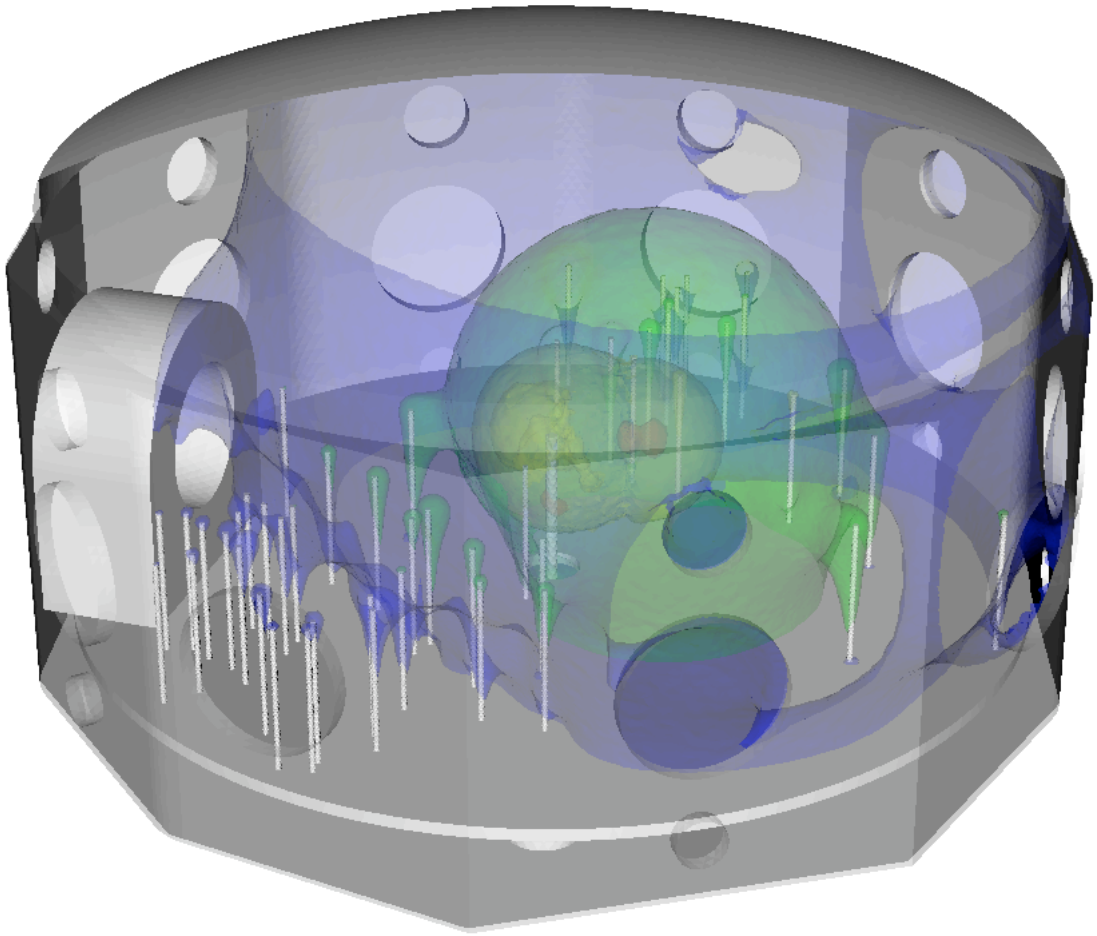

Figure 7: Contours of the electric fields (log scale) in the Titan chamber after divergence cleaning. The blue and green contours are unphysical.

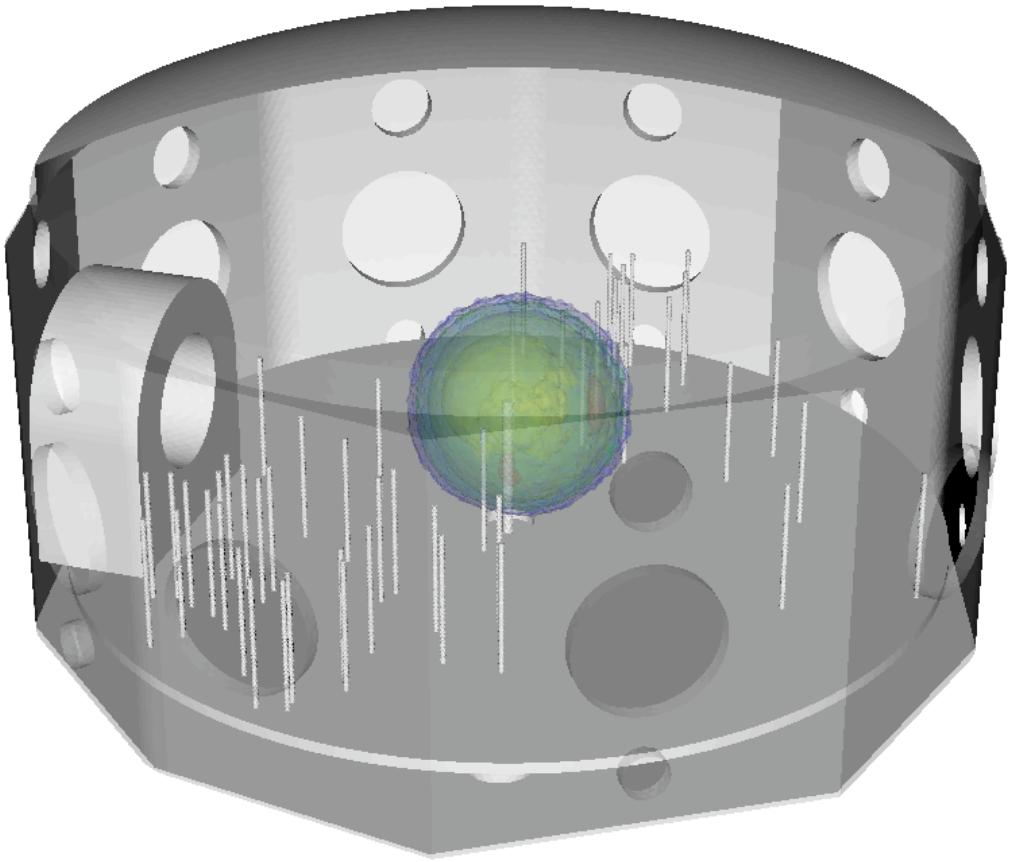

Figure 8: Contours of the electric fields (log scale) in the Titan chamber with new D/H formulation. There are no unphysical fields. The highest strength contour (red) on right side is associated with an electron bunch leaving the target.

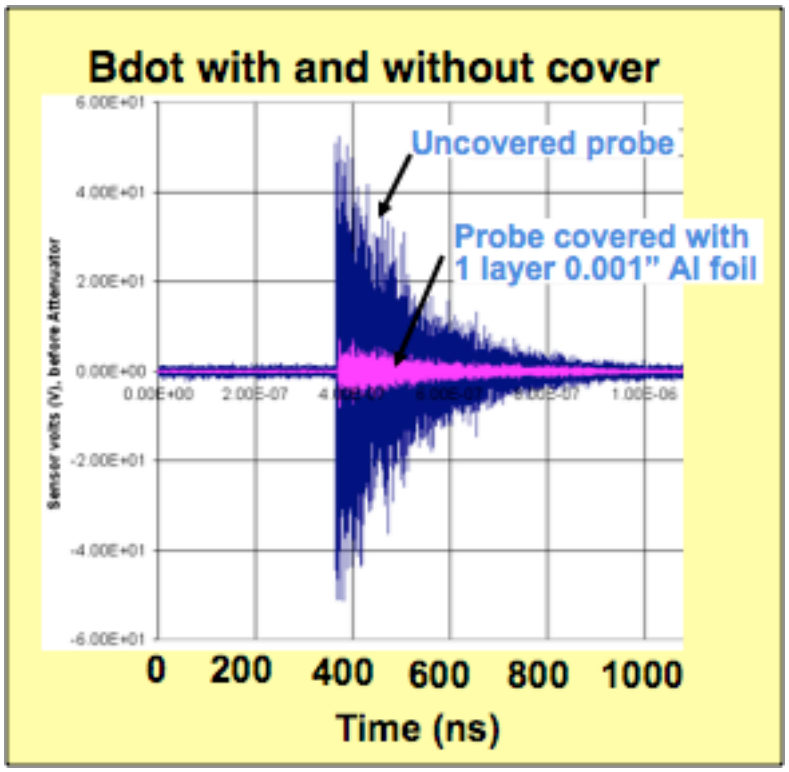

Figure 9: Scope trace of high-frequency B-dot probe uncovered and covered to measure effect of noise in cables and scope.

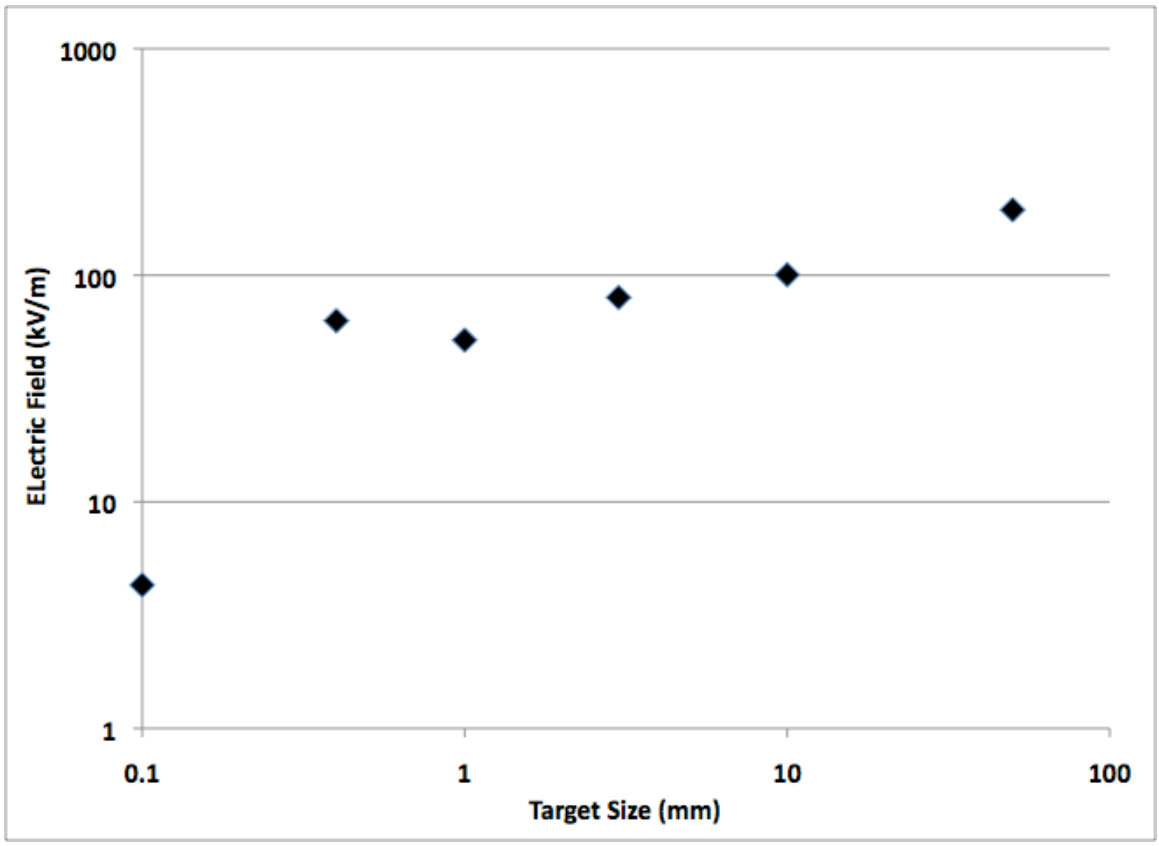

Figure 9: The peak electric field strength measured by D-dot probe out to 2 GHz as a function of target size.

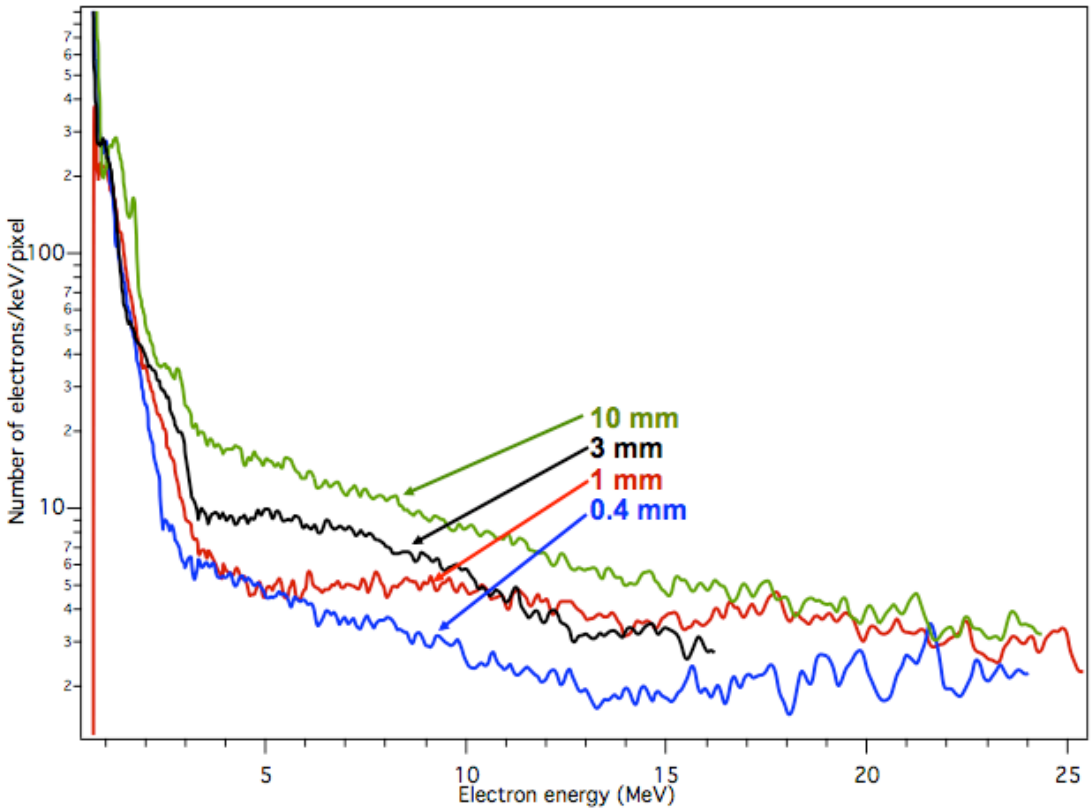

Figure 11: The spectrum of escaping electrons measure by compact high-energy spectrometer for 4 targets with different sizes.

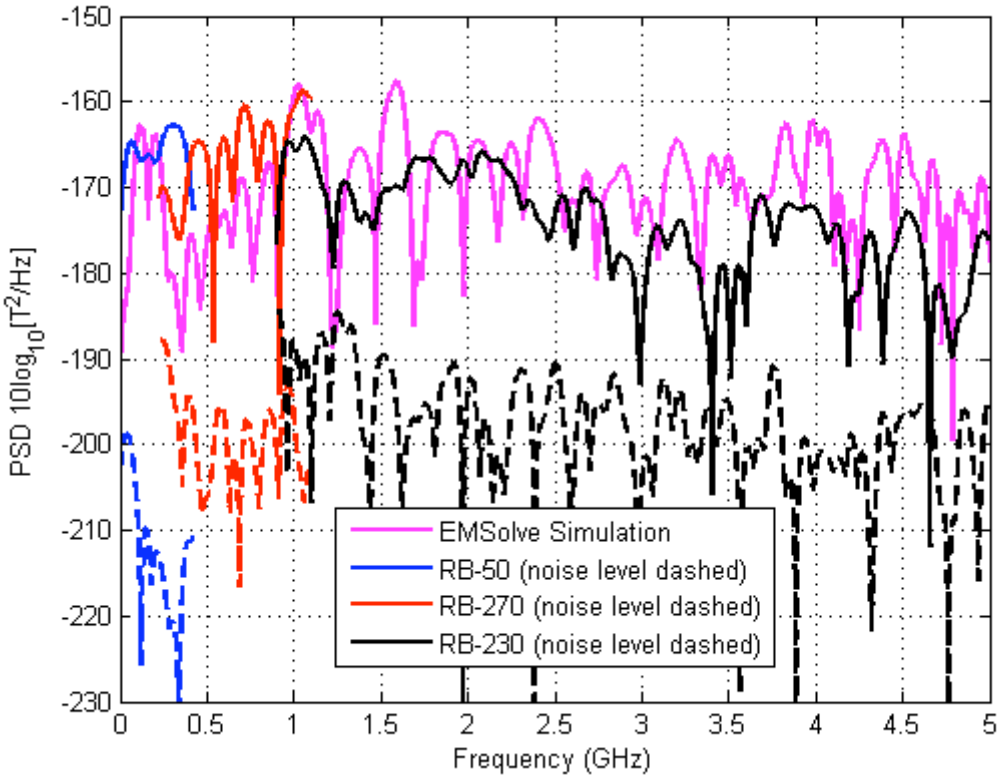

Figure 12: The EMP power spectral density as a function of frequency. Combine data from low-frequency (RB-50), mid-frequency (RB-270), and high-frequency (RB-230) Prodyn B-dot probes. Noise levels are given as dashed lines. Result of simulation using EMSolve with 5 x 10^{12} escaping electrons is also shown.

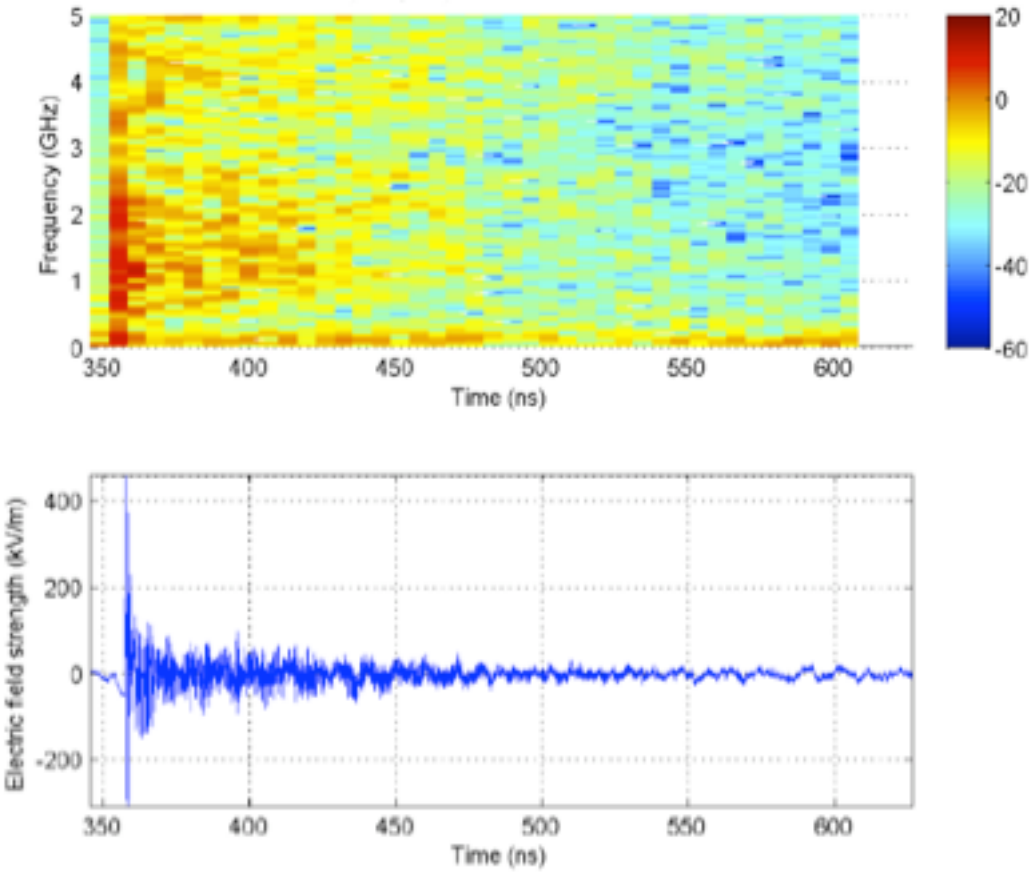

Figure 13: The lower plot is the calculated electric field strength as a function of time, which is obtained from the rate of change of the magnetic field as a function time measured by a high-frequency B-dot probe in the vertical orientation assuming free-space ratio between fields. The upper curve is the frequency dependence of fields as a function of time.

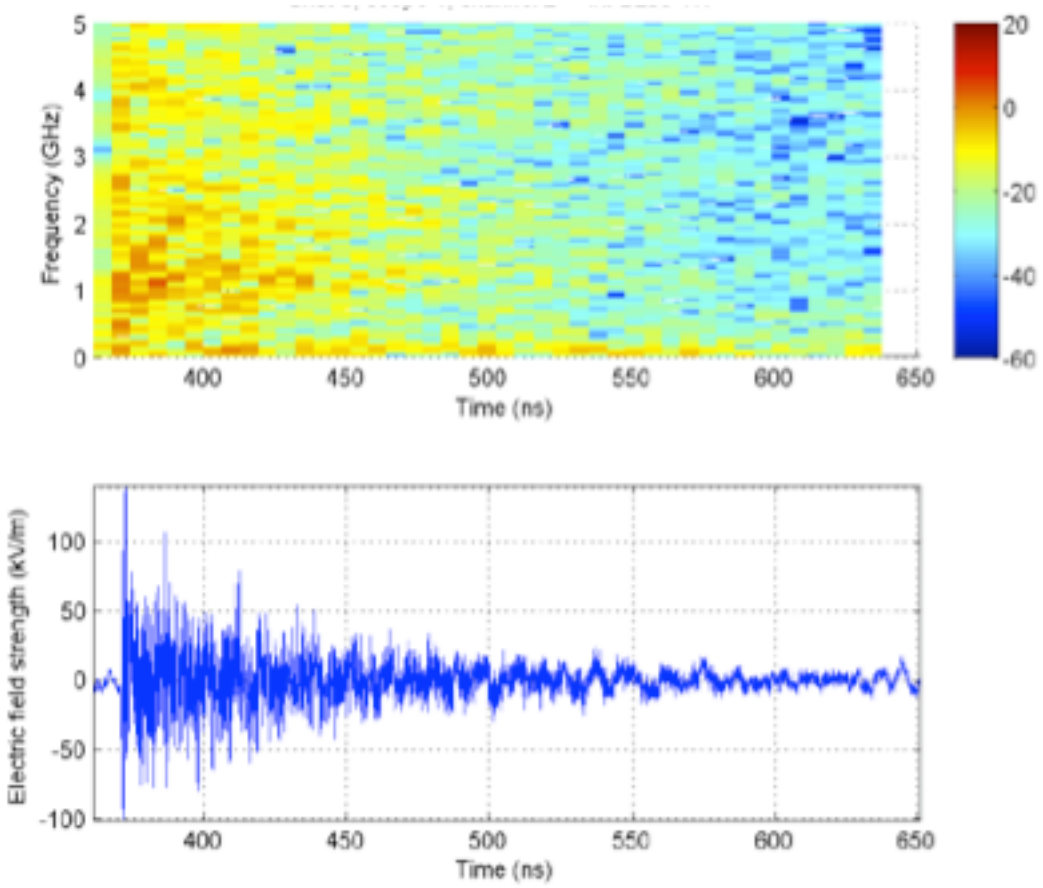

Figure 14: Results similar to what is shown in Figure 11, except that the fields are measured by a B-dot probe in the horizontal orientation.

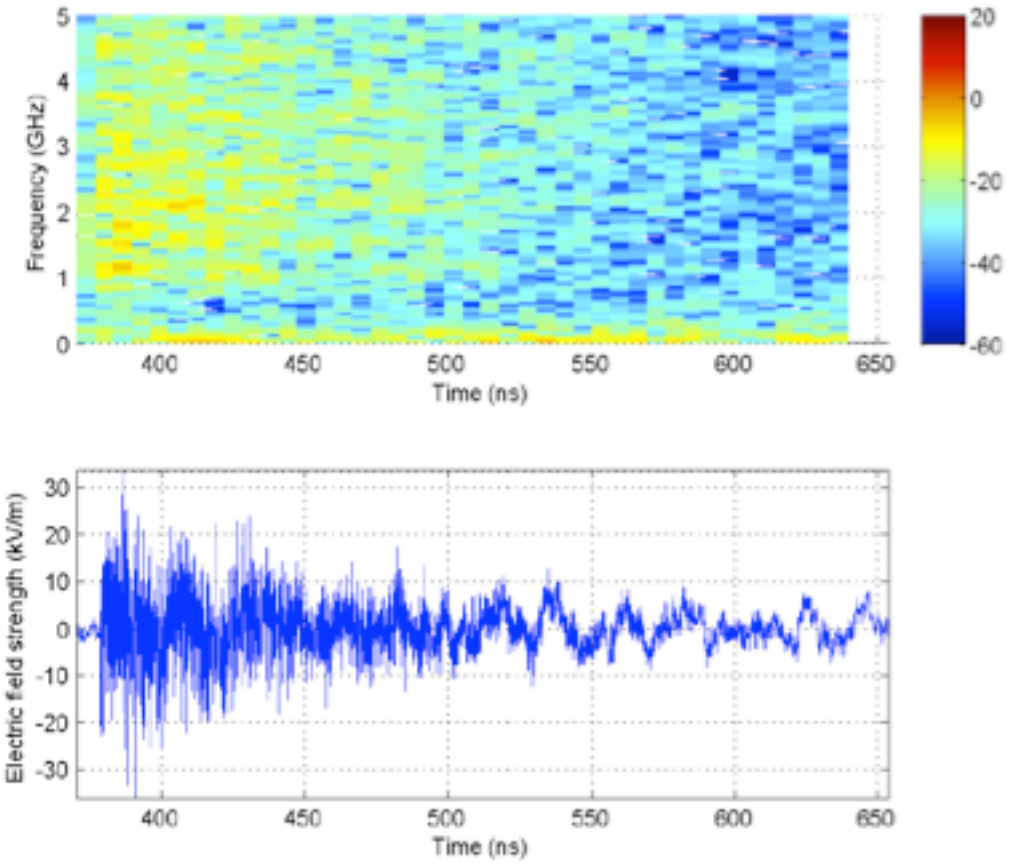

Figure 15: The lower curve is the electric field as a function time measured by a B-dot probe located outside the chamber near a window port. The upper curve is the frequency dependence of the field as a function of time.

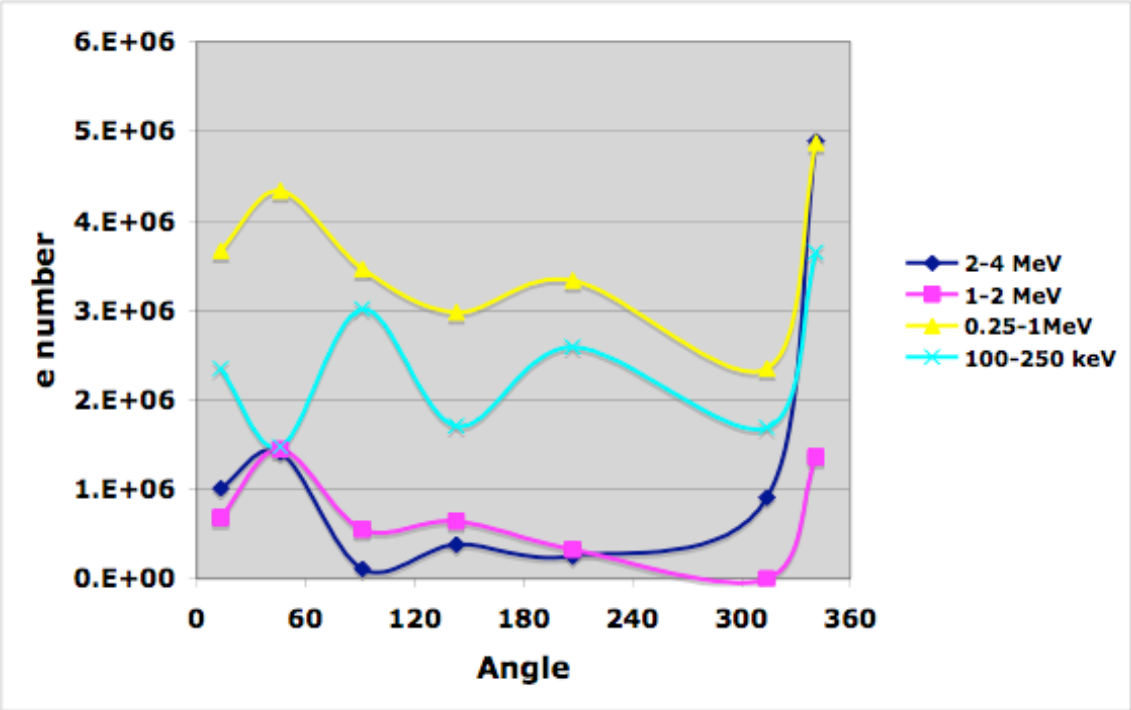

Figure 16: The angular dependence of escaping electrons in four energy bins measured by 7 compact electron spectrometers. The laser axis is at 0 degrees and the normal to the back surface of the target is at an angle of 332 degree.

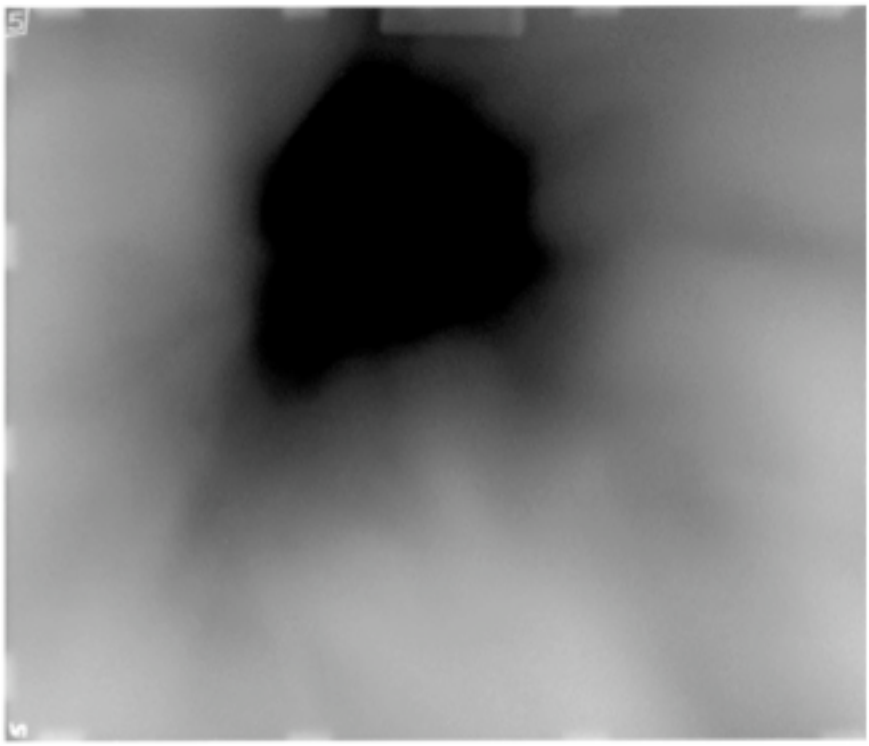

Figure 17: Evidence of an electron beam leaving the rear surface of the target and striking the large image plates.

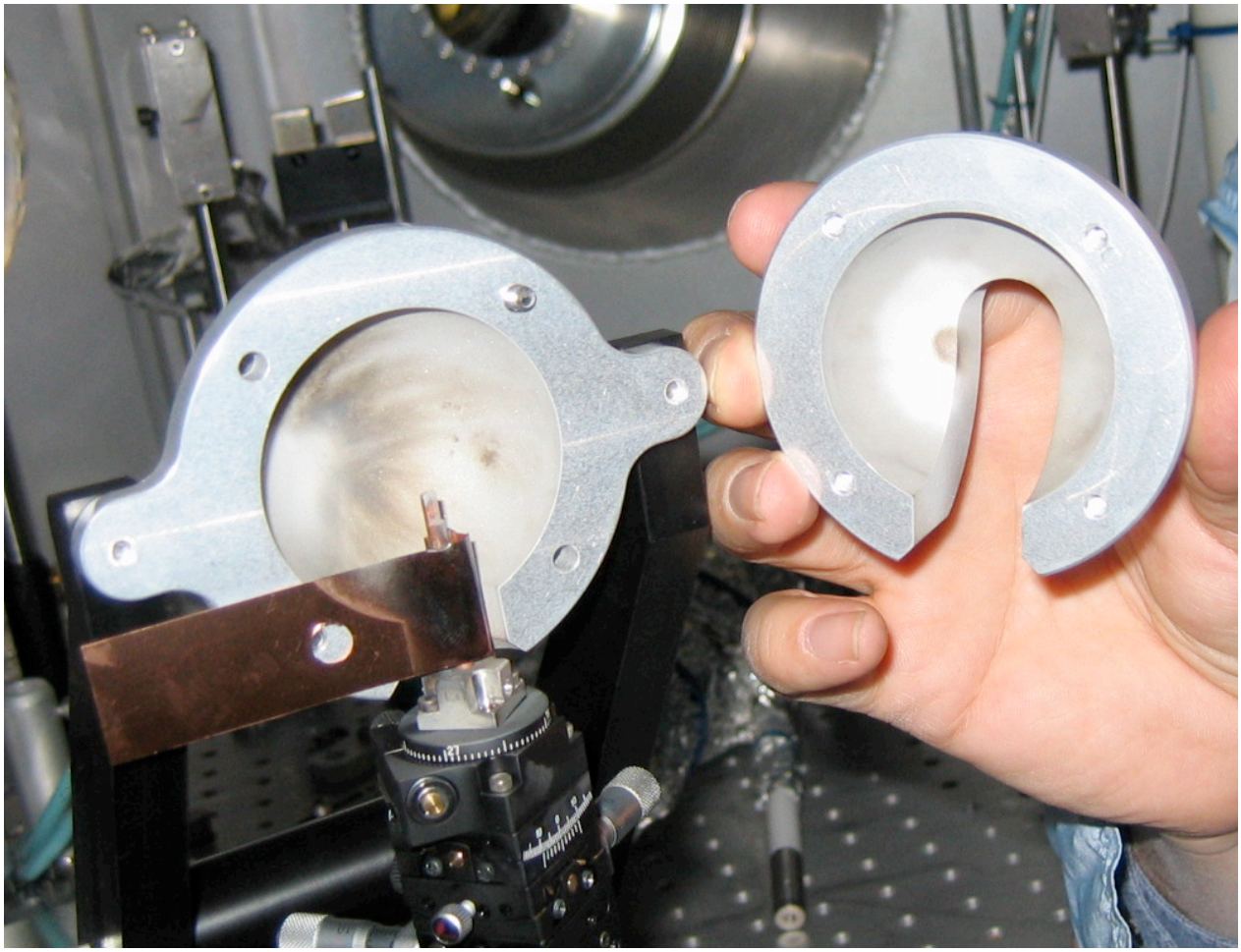

Figure 18: A spherical electron beam dump is shown including a Cu foil that provides a low impedance path to the target. The opening slit in the sphere for the target holder and laser beam is shown.

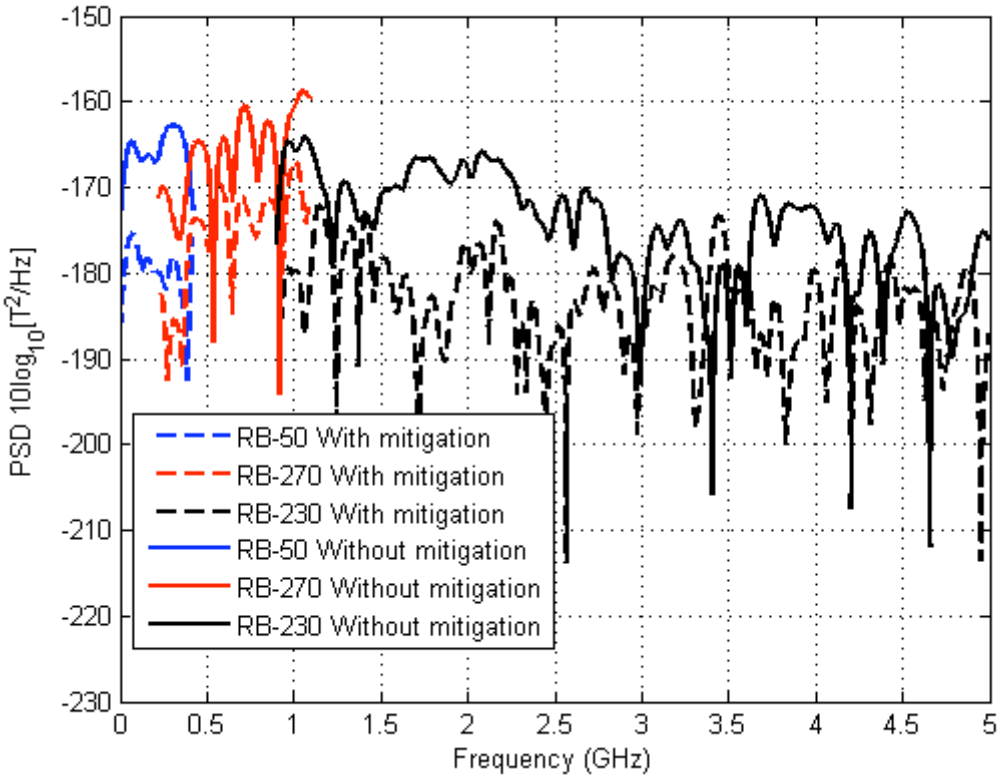

Figure 19: The EMP power spectral density measured by 3 B-dot probes for a target with and without a mitigation sphere surrounding the target.

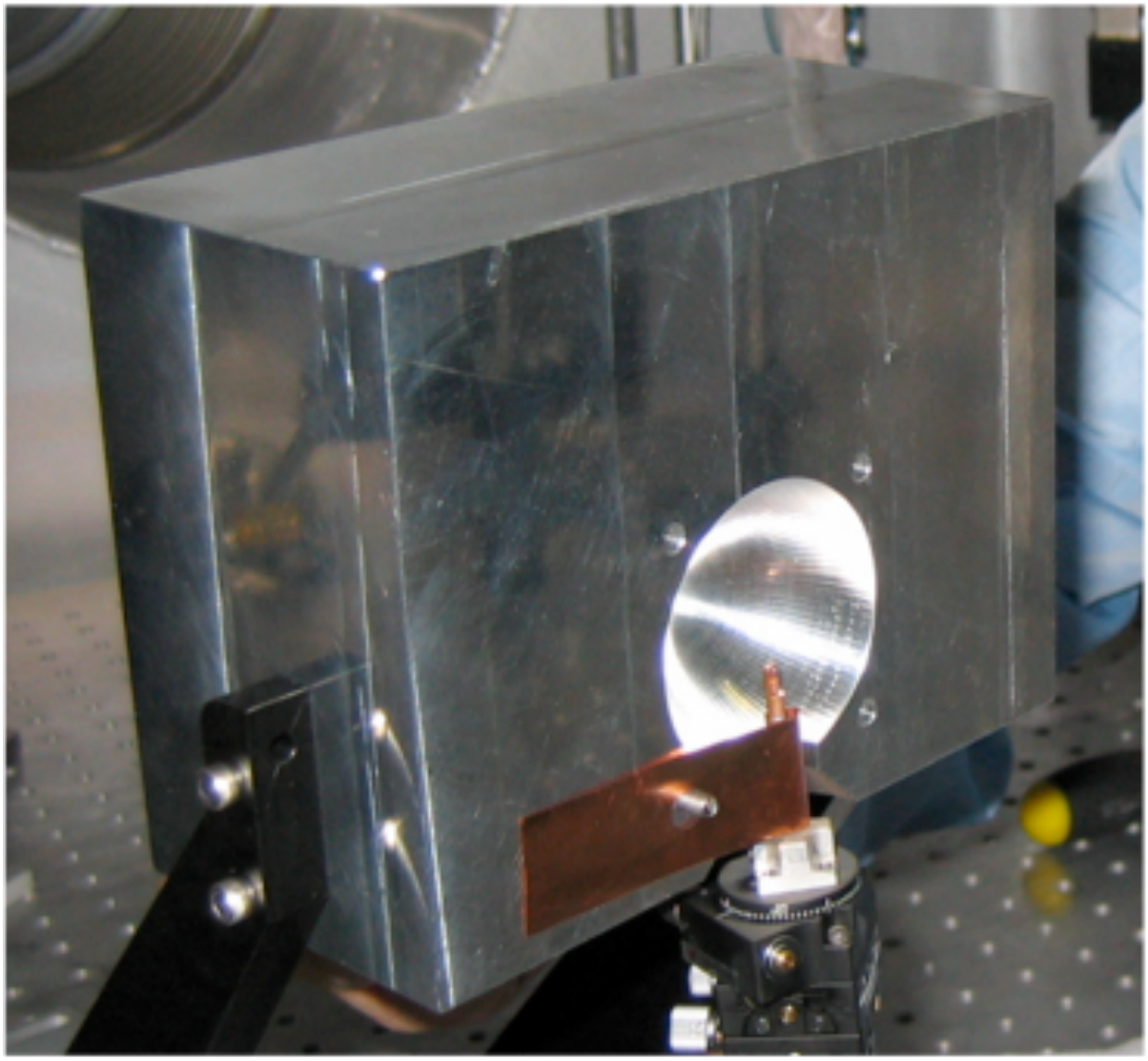

Figure 20: One half of the mitigation cube that is thick enough to block essentially all the escaping electrons.

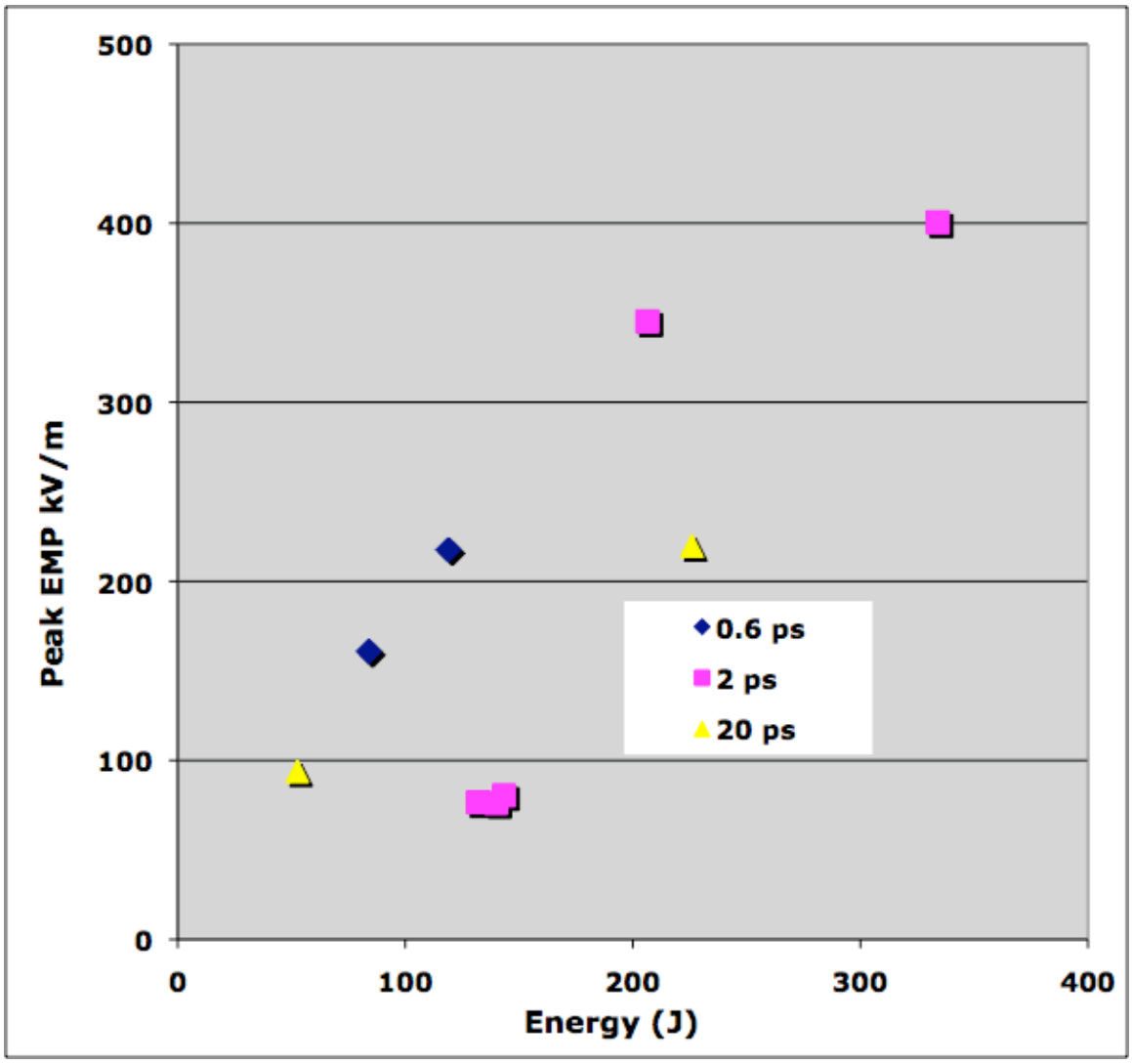

Figure 21: The dependence of the peak EMP electric field strength as a function of energy for three different laser pulse durations.